INTERNATIONAL JOURNAL OF MARITIME TECHNOLOGY

IJMT Vol.19 / Winter & Spring 2024 (43-56)

Available online at: www. ijmt.ir

A Process-based calibration Procedure for Non-Cohesive Silt Transport Models at Shahid Rajaee Port Access Channel

Seyed Mojtaba Hoseini Chavooshi [1], Ulrich Reza Kamalian [2*]

[1] *PhD Candidate, Civil Engineering Department, University of Qom; sm.hoseini@stu.qom.ac.ir*

[2] *Assistant Professor, Civil Engineering Department, University of Qom; ur.kamalian@qom.ac.ir*

ARTICLE INFO

Article History:
Received: 17 Aug 2023
Accepted: 28 Feb 2024
Available online: 01 May 2024

Keywords:

Mud Transport
Suspended sediment transport
Channel siltation
Model calibration
Shahid Rajaee Port

ABSTRACT

Numerical modeling is the most common approach for predicting harbor channel siltation. It requires a comprehensive calibration process because there are several calibration parameters. The most crucial criterion for model calibration is suspended sediment concentration (SSC). The agreement between the measured and simulated SSC time series is usually verified based on generic statistical parameters such as RMSE and R^2. This method does not address the important phenomena related to channel siltation; for instance, the siltation rate during neap and spring tidal cycles cannot be distinguished in such manner. A process-based calibration procedure has been proposed in this paper which considers some criteria facilitating the calibration processes. Based on analyzing the measured turbidity and current speed data, some criteria were established which convey underlying phenomena affecting sediment transport. They are: (1) the difference between maximum SSC (or turbidity) at neap and spring and (2) at ebb and flood tide, (3) the minimum turbidity at slack water during spring tide, and (4) the current speed-SSC (or turbidity) regression curve. The proposed procedure has been used to calibrate channel siltation in a real case study: Shahid Rajaee port access channel located in the Khoran strait, Iran. As the underlying phenomena affecting sediment transport was considered, the number of simulation runs for calibration processes were considerably decreased.

1. Introduction

Prediction of harbor channel sedimentation has always been of considerable interest to coastal engineers. Modeling approaches ranging from simplified models [1, 2, 3] to sophisticated physics-based models [4, 5, 6, 7] are comprehensively adopted. Numerical models need to be thoroughly calibrated based on measured data. "Calibration is the process of tuning all parts of the model system based on local data and common sense" [8]. Calibration of sediment transport models (especially in areas with silt) is a relatively complex procedure. It often requires long-term detailed measured data. A process-based method has been proposed in this paper for calibrating non-cohesive silt models in tidal channels.

Suspended sediment transport is the most essential phenomenon for sediment transport in silt environments. Usually, numerical models based on mass and momentum conservation equations are used to predict suspended load (Some researchers have employed artificial neural network (ANN) models [9, 10, 11, 12, 13, 14, 15, 16, 17] or hybrid models (combination of numerical and ANN models) [18, 19, 20]). Numerical models contain some calibration parameters which need to be tuned based on available field data.

Non-cohesive silt models are usually calibrated to SSC. This approach has been adopted extensively by coastal engineers. Lumborg and Windelin [21] modeled the hydrodynamic and sediment transport of the Romo Dyb tidal area using the numerical model MIKE 21 MT (Mud Transport). They calibrated the sediment transport model through comparison of the time-series of measured and simulated SSC. There was not a great similarity between the time-series. However, the modeled and measured suspend SSC patterns were in good agreement. Lumborg and Pejrup [22] used MIKE 21 MT to calculate the annual net transport of fine sediment for the Lister Dyb tidal area in the Wadden Sea. The model was calibrated using directly measured critical bed shear stress by the EROMES instrument. They used the timing of re-suspension events as a validation parameter. Lopes et al. [23] studied the dynamics of suspended sediment in the Ria de Aveiro

lagoon with the numerical model HSCTM (Hydrodynamics, Sediment and Contaminant Transport Model). The measured and simulated yearly average SSC was compared to calibrate the model. The results proved that settling velocity and bed erodibility are the most important parameters for accurate model calibration. Margvelashvili et al. [24] employed a one-dimensional transport model in the Torres Strait region of northern Australia. Calibration parameters including critical bed shear stress for erosion, settling velocity, and bed roughness were calculated for each time step as time-series data. The calibration parameters were not constant with time. Therefore, they increased the number of sediment fractions to reach a nearly constant value in time for each calibration parameter. Ganju and Schoellhamer [25] studied the long-term morphodynamics of a tidal estuary with a narrow entrance. They used sediment flux at the entrance as the calibration criterion. Xie et al. [26] calibrated the 2D depth-averaged MIKE 21 MT model to the yearly representative SSC rather than time-series data. The SSC was proved to be dependent only on the local wave characteristics because of the limited tidal velocity. The yearly representative sediment concentration was selected as the criterion. Erikson et al. [27] simulated sediment exchange at the tidal-dominated Golden Gate inlet. The morphological changes were simply dependent on suspended sediment flux across the Golden Gate inlet. The model was calibrated based on the relationship between water discharge and suspended sediment flux across the inlet. Using the Delft3D numerical model, Tu et al. [28] calculated morphodynamic changes in estuaries and coastal zones of the Mekong Delta. Due to the shortage of SSC measured data, the calibration process was limited to a qualitative comparison of the order of magnitudes of the measured and simulated SSC. The depth-averaged SSC has been considered in this regard. Chang et al. [29] used the Coupled-Ocean-Atmosphere-Wave-Sediment Transport model (COAWST) to estimate sediment transport patterns and morphodynamic changes in the Nakdong Estuary. Measurement showed that the SSC was distributed uniformly. Therefore, the depth-averaged SSC was established as the criteria for model calibration. The model performance was evaluated using correlation coefficient and mean relative error. The changes of SSC in each tidal cycle were neglected because sediment transport inside the estuary was dominated by river discharge. Xiao et al. [30] used the finite-volume community ocean model (FVCOM) to simulate sediment transport patterns in the Sydney Harbor Estuary. To evaluate model performance, they compared measured and simulated near-bed SSC. Zhua et al. [31] estimated sediment transport time scale in the Modaomen Waterway using a three-dimensional numerical model named Environmental Fluid Dynamics Code (EFDC) to determine the retention time of pollutants absorbed by sediment. The model calibration was performed using Skill Score [32] and Correlation Coefficient as the calibration criteria. Orseau et al. [33] simulated the morphology of the Gironde Estuary using the SISYPHE model. They conducted a calibration of the model with respect to SSC. The comparison between the measured and simulated SSC data revealed a high level of agreement, although the model results underestimated the measured data. Bitencourt et al. [34] studied the seasonal and annual variability of SSC in The Patos Lagoon, Brazil, using SISYPHE model. The calibration processes involved a comparison between simulated and in-situ measured SSC data, revealing a generally good agreement for the majority of the time. Fagundes et al. [35] used suspended sediment concentration (SSC), water quality and remote sensing data to calibrate a large-scale sediment model. The results showed that the spectral surface reflectance, total suspended solids and turbidity data can enhance the performance of sediment models. Shanesazzadeh and Ardalan [36] studied the sediment transport and morphological processes in the Khoran Strait. Both conceptual and 2d numerical model (MIKE21) were applied to define the origin of the sediment. The results indicated that the main sediment sources are sediments suspended from the bed. The calibrated model was also used to estimate the morphological changes of Rajaee port access channel. The model results were compatible with measured data. Jafarzadeh Dehkordi, and Ershadi [37] studied the sedimentation processes in the Shahid Rajaee port access channel. They calibrated the MIKE 21 ST model to SSC measured data. The calibrated model was used to estimate the sedimentation rate and pattern in the access channel. Results indicated that the sedimentation rate in the middle of access channel is higher compared to other parts of the channel. Lisboa et al. [38] employed the SISYPHE model to investigate erosion and deposition processes in the Río de la Plata and Patos Lagoon. They compared the measured and simulated SSC, observing that while the simulated SSC generally overestimated the measured data, the model results effectively captured the main patterns of the measured data.

The difference between erosion/deposition at neap and spring tidal cycles, the main cause of fine sediment transport, has not been the subject of previous studies. Erosion, suspended sediment transport, and channel siltation at spring tidal cycles are usually higher than at the neap. The purpose of this research is to develop a process-based procedure for calibration of silt transport models in corresponding situations. To this end, seven specific criteria are established to compare field measurements with model results. The aim is to

decrease the number of test simulations as much as possible.

2. Study Area

The study area is Shahid Rajaee port, located at the Khoran strait within the strait of Hormoz, Persian Gulf (Fig. 1). The port handles nearly 100,000,000 tons of cargo annually. It is designed for vessels with a capacity of 150,000 tons. The water depth in the access channel is 15 meters. The port has a development plan which includes increasing the access channel depth up to 19 meters. The predominant sediment type in the area is non-cohesive silt. The tidal current at the strait is asymmetric. Fig. 2 shows the instantaneous measured current and water level for a month with the maximum ebb and flood tidal current equal to 1.1 and 0.9 $m.s^{-1}$, respectively. The phase difference between current speed and water level is considerable. There is no significant wave because of the sheltering effect of Qeshm Island. Therefore, tidal current is dominant for sediment transport processes. According to admiralty tide table, the study area experiences a semi-diurnal tidal cycle. It is located at a macro-tidal environment whose tidal range increases along the strait from east to west because of complex bed topography (see Table 1). Tidal levels of study area are also schematically depicted in Fig. 3.

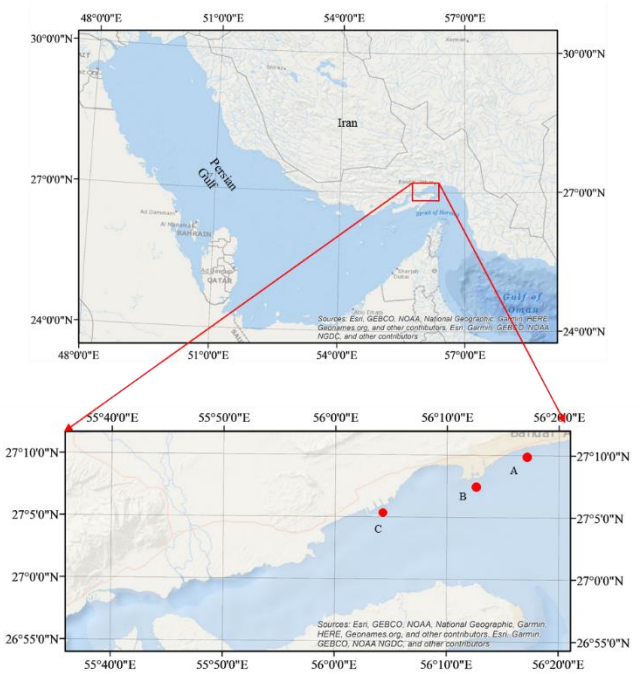

Fig. 1. The study area; red circles show the locations where tidal levels have been measured.

Table 1. Tidal levels of the study area (red circles in Fig. 1) [39]

Sta	Position (UTM 40)		HAT (m)	MHWS (m)	MHWN (m)	MLWN (m)	MLWS (m)	LAT (m)
	X (m)	Y (m)						
A	429000	3005098	3.8	3.4	2.6	1.4	0.7	-0.1
B	420720	3001455	4.0	3.6	2.9	1.5	0.7	-0.3
C	407478	2997854	4.2	3.7	2.9	1.5	0.6	-0.4

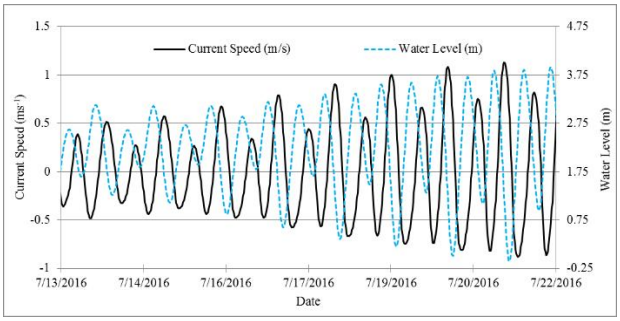

Fig. 2. The time series of water level (relative to MSL) and current velocity for a month (measured at 27.054° Lat 56.027° Lon) [40]

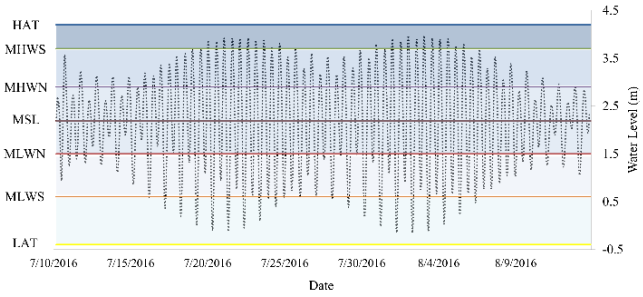

Fig. 3. Tidal levels in the study area

The access channel is nearly 6 to 9 meters deeper than the natural depth of the study area. Therefore, it acts as a sediment trap. Previous studies [40, 41, 42] have estimated the annual sedimentation in the access channel in the range of 80,000 to 120,000 m^3 based on dredging data and comparison of successive hydrographies. The value 120,000 m^3/year is used for model calibration.

3. Materials

3.1. Bathymetry

Fig. 4 shows the bathymetry of the study area. There are several submerged branches parallel to the tidal flow, which affect the flow field.

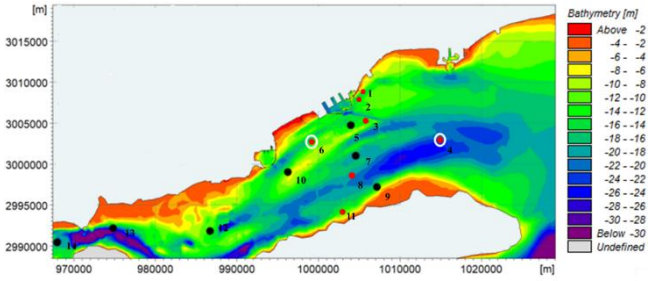

Fig. 4.The Bathymetry and the location of SSC (black dots), current speed (red dots), and turbidity (white dots) measurement stations (UTM39)

3.2. Sediment Data

SSC has been measured for 25 hours at each station in January 29th 2008, but only the minimum, maximum, and average values of five stations are available, which are given in Table 2. The location of measurement stations is shown in Fig. 4. The water samples at each station were taken at 6 distances from water level which are not equidistant, 2 points from the water surface to mid depth and 4 points from mid depth to bed level. The SSC was measured via Filtration method.

Table 2. The minimum, maximum, and average SSC values at some stations (g.m^{-3}) [40]

Sta	Position (UTM40)		Spring			Neap		
	X (m)	Y (m)	Min	Max	Avg	Min	Max	Avg
5	408635	2994996	50	80	70	50	70	60
7	409253	2991000	50	90	60	40	70	50
10	399710	2989122	60	110	70	50	60	50
12	389923	2982727	70	140	90	40	150	60
13	377523	2983471	80	160	110	50	70	60

In the study area, sediment type is mainly non-cohesive silt. However, near the coastline are some areas with coarser grain size. As the harbour entrance is locally affected by dredging operation, coarse sand also exist in this area. The sediment size in the study area is condensed in Table 3.

3.3. Hydrodynamics and Turbidity Field Measurements

Two comprehensive field measurements have been accomplished in the strait [40, 43]. Current speed has been measured continuously in seven stations for one to three months (see Table 4). Turbidity has also been measured in two stations (4 and 6) for one month, with simultaneous current speed measurement. The location of measurement stations are shown in Fig. 4.

Table 3. Sediment grain size at the study area [40]

Position (UTM40)		Bed Level m (CD)	D_{50} (mm)	Clay (%)	Position (UTM40)		Bed Level m (CD)	D_{50} (mm)	Clay (%)
X (m)	Y (m)				X (m)	Y (m)			
412122	3002309	+1.5	0.138	0	405144	2996147	-5	0.013	5
412152	3002117	0	0.026	5	403846	2996668	+1.5	0.557	0
412249	3002018	-2	0.032	6	404080	2996009	0	0.116	0
412883	3000768	-5	0.026	5	404147	2995888	-2	0.144	5
409605	2998945	+1.5	0.574	0	404194	2995799	-5	0.157	5
409702	2998911	0	0.186	0	400619	2995330	+1.5	0.058	5
409776	2998843	-2	0.027	2.5	401269	2994164	0	0.104	2
409836	2998766	-5	0.064	2.5	401289	2994119	-2	0.142	2
409369	2998457	-2	0.012	6	401663	2993390	-5	0.116	5
409421	2998403	-5	0.013	5	411400	2995600	-17.5	0.015	10
407825	2996563	-15	0.007	5	414596	2994802	-20	0.15	10
406983	2997605	-13	0.008	10	408104	2996244	-20	0.6	5
404793	2997156	+1.5	0.277	0	402389	2994822	-2.5	0.1	0
405129	2996273	-2	0.099	5	396758	2988818	-13	0.1	10

Table 4. Depth and method of current speed measurement and type of instrument [40]

Sta	Position (UTM40)		Water depth (m)	Instrument model	Measurement distance from the bed (m)	Frequency and time averaging of records	Time interval between records (min)	Measurement duration
	X (m)	Y (m)						
1	411611	2999308	11	AWAC (Nortek AS)	Multiple (with 1m intervals)	2Hz – 120s	10	7/8/2007 to 9/9/2007
2	410899	2998043	7	AWAC (Nortek AS)	Multiple (with 1m intervals)	2Hz – 120s	10	9/1/2008 to 24/1/2008

3	411232	2995450	8	ADCP Mini Sontek	Multiple (with 1m intervals)	2Hz – 120s	10	12/10/2009 to 12/1/2010
4	418709	2992507	20	RCM9 MKII Aanderaa	10	120s	10	5/9/2007 to 10/9/2007
6	403448	2992927	10	RCM9 MKII Aanderaa	7	120s	10	8/8/2007 to 4/9/2007
8	408143	2988756	15	ADCP Argonaut Sontek	Multiple (with 1m intervals)	2Hz – 90s	20	13/10/2009 to 12/1/2010
11	407340	2988756	4	ADV Hyra Sontek	2.5	2Hz – 120s	30	9/10/2009 to 10/11/2009 10/12/2009 to 13/1/2010

4. Methodology

The model Mike 21 coupled Flow and Mud Transport on flexible mesh has been used in this study. The simulation aims to estimate the increase in the access channel sedimentation due to the increase in its depth.
The two-dimensional depth-averaged Navier-Stokes (Reynolds-averaged) equations are used for flow field simulation with the Smagorinsky formula for turbulent eddy viscosity. The hydrodynamic module has formerly been calibrated. This paper does not focus on the hydrodynamic model calibration.
Sediment transport is calculated through a two-dimensional advection-diffusion equation (Eq. (1)) [4]

$$\frac{\partial \bar{c}}{\partial t} + u\frac{\partial \bar{c}}{\partial x} + v\frac{\partial \bar{c}}{\partial y} = \frac{1}{h}\frac{\partial}{\partial x}\left(hD_x\frac{\partial \bar{c}}{\partial x}\right) + \frac{1}{h}\frac{\partial}{\partial y}\left(hD_y\frac{\partial \bar{c}}{\partial y}\right) + Q_L C_L\frac{1}{h} - S \quad (1)$$

where $\bar{c}$ is depth-averaged concentration ($g.m^{-3}$); u and v are components of depth-averaged flow velocities in x and y directions, respectively ($m.s^{-1}$); D_x and D_y are dispersion coefficients in the x and y directions, respectively ($m^2.s^{-1}$); h is water depth (m); Q_L is source discharge per unit horizontal area ($m^3.s^{-1}.m^{-2}$); C_L is concentration of the source discharge ($g.m^{-3}$); and S is deposition/erosion term ($g.m^{-3}.s^{-1}$).
Eq. (2) to Eq. (4) are used to calculate deposition and erosion rates [4].

$$S_d = W_s.c_b.P_d \quad (2)$$

$$P_d = 1 - \frac{\tau_b}{\tau_{cd}} \quad (3)$$

$$S_e = E\left(\frac{\tau_b}{\tau_{ce}} - 1\right)^n \quad (4)$$

where W_S is settling velocity ($m.s^{-1}$); c_b is the near-bed concentration ($kg.m^{-3}$); P_d is the probability of deposition; τ_b is the bed shear stress ($N.m^{-2}$); τ_{cd} and τ_{ce} are critical bed shear stresses for deposition and erosion, respectively ($N.m^{-2}$); E is erodibility coefficient of bed ($kg.m^{-2}.s^{-1}$); n is power of erosion; and S_e and S_d are bed erosion and deposition rates ($kg.m^{-2}.s^{-1}$).
The model uses empirical formulas for the SSC profile because it is a 2-dimensional depth-averaged model.
Setup and calibration parameters for suspended sediment transport modeling are settling velocity, critical bed shear stress for erosion and deposition, bed roughness, erodibility coefficient of bed, and power of erosion formula. Relative humidity, consolidation, flocculation, and hindered settling velocity are crucial in cases wherein sediment is cohesive, which is not the case in this study. Seven criteria have been proposed to determine the mentioned parameters. They are the consistency between the measured and simulated data for: (1) the order of magnitude of simulated and measured SSC, (2) the minimum turbidity at slack water during spring tide, (3) the difference between maximum turbidity at neap and spring tide, (4) the difference between maximum turbidity at ebb and flood tide, (5) the minimum current speed required for initial suspension of sediment, (6) the slope of current speed
(velocity)-SSC regression curve, and (7) the deposition rate in the access channel.
Each criterion is mainly affected by one or two calibration parameters. Moreover, each of them conveys a particular physical phenomenon. The effect of each calibration parameter on dominant phenomena is assessed using the criteria. The second criterion demonstrates if the suspended sediments have enough time to settle at slack water during spring tide. It also shows the source of suspended sediment (tidal cycles or river flood events). The third criterion demonstrates the contribution of neap and spring tide to access channel deposition. The fourth criterion shows the net direction of sediment transport. The fifth criterion determines the critical bed shear stress for erosion, which is highly dependent on the minimum current speed required for initial suspension. The sixth criterion is used to determine the coefficient and power of erosion formula (Eq. (4)).
The first criterion is controlled using Table 2. The second, third, and fourth criteria are checked using the comparative time series of current speed and turbidity

(Fig. 5). The fifth and sixth criteria are controlled using the scatter plot of velocity-SSC (Fig. 6). The suspension start from the point where a slight increase in current speed leads to a rapid growth in turbidity (red circles in Fig. 6). Figs. 5 and 6 illustrate sample graphs of current speed and turbidity based on measurement at station six in the study area (the nearest point to the access channel).

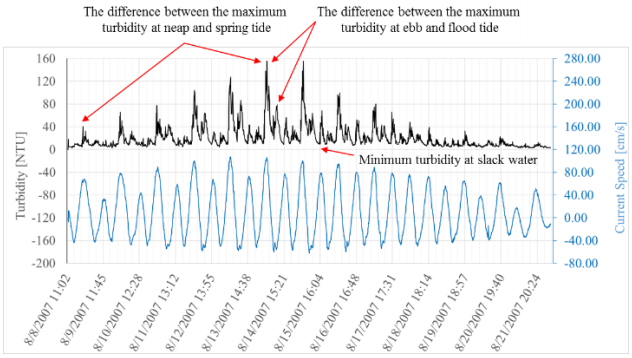

Fig. 5. The comparative time series of measured current speed and turbidity at station six at mid-depth (see Fig. 4)

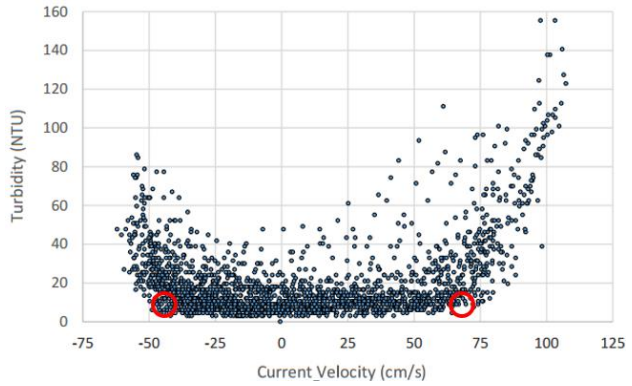

Fig. 6. The correlation between measured current speed and turbidity at station six at mid-depth (see Fig. 4); red circles show the critical current speed for suspension.

The proposed procedure for the calibration process is as follow:

(a) Set the critical bed shear stress for erosion based on the minimum current speed required for suspension.

(b) Approximate the settling velocity and critical current speed for deposition based on the first criterion.

(c) Set the settling velocity and critical current speed for deposition based on the second, third, and fourth criteria.

(d) Set the erodibility coefficient and power of erosion formula (Eq. (4)) based on the sixth criteria (see Fig. 6)

(f) Fine-tune all calibration parameters regarding the last criteria

4.1. Hydrodynamic Model Calibration

Calibration of the hydrodynamic model is the prerequisite for accurate calibration of the sediment transport model. In this study, the results of a calibrated hydrodynamic model have been used. The hydrodynamic model includes two parts: (1) a regional model including the Persian Gulf and Oman Sea and (2) a local model including the Hormoz and Khoran strait (Figs. 7 and 8). The regional model was calibrated to water level at 10 points in the Persian Gulf. The maximum difference between measured and simulated water level was 20 cm, and the average value of R^2 was 0.97.

The local model receives boundary conditions from the regional model. An unstructured mesh with 10582 nodes is used for the local model. The distance between nodes in the vicinity of the access channel is in the range of 90 to 200 meters. The bed resistance type is Manning number with value of 50 $m^{1/3}/s$. The Smagorinsky formulation is used for eddy viscosity, and the constant value is set to 0.28.

Fig. 7. The domain of the regional model; red lines show the boundaries of the local model

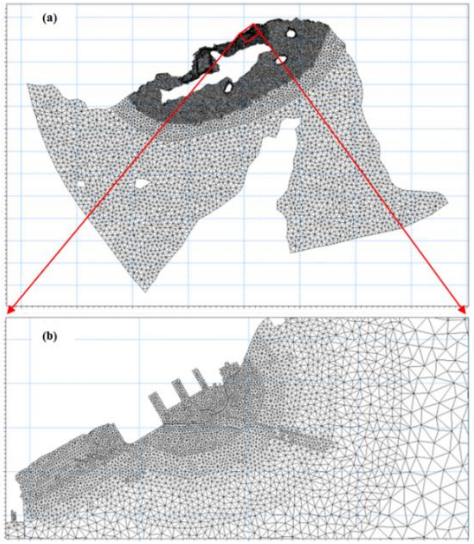

Fig. 8. The domain of the local model

The local model was calibrated to water level and current speed at two stations in the Khoran strait. Fig. 9 shows the time series of measured and simulated current speed at station six. The values of RMSE and

R^2 are 0.26 $m.s^{-1}$ and 0.97, respectively, which confirms the good agreement between measured and simulated data.

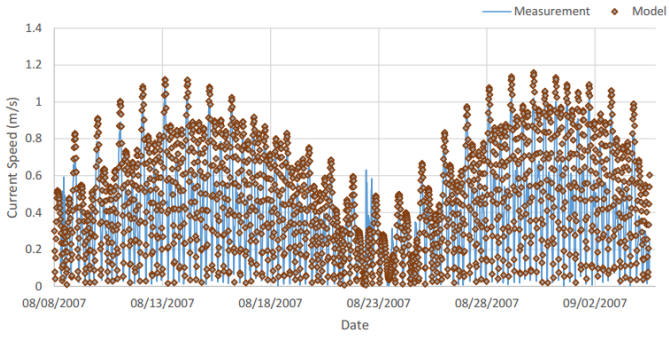

Fig. 9. Comparison of measured and simulated current speed at station six

4.2. Silt Transport Model Calibration

Essential calibration parameters are (1) Settling velocity, (2) critical bed shear stress for deposition, (3) critical bed shear stress for erosion, (4 and 5) coefficient and power of erosion formula, and (6) bed roughness. Considering non-cohesive sediment, calibration parameters related to consolidation are not effective. 41 simulation scenarios have been applied for sediment transport model calibration. The hydrodynamic part takes a long time, while the suspended sediment transport simulation is relatively fast. MIKE 21 Flow model has an option that enables the user to simulate several sediment transport scenarios based on the existing hydrodynamic model output. In this study, the sediment transport model was run solely based on the results of the calibrated hydrodynamic model. In this way, the simulation time for each scenario was just about 10 minutes on a system using Core (TM) i7-4702 MQ CPU @ 2.2 GHz.

Measured turbidity data at station six (see Fig. 4) is used for model calibration. It is the nearest station to the access channel and located on the streamline which crosses the channel. Fig. 5 and 6 illustrate the relation between the current speed and turbidity. Due to the shortage of available SSC field data, turbidity data has been used to calibrate the sediment transport model. It worth noting that there is a direct correlation between turbidity and SSC especially in low-turbidity waters [44, 45, 46, 47, 48, 49, 50, 51, 52], which is similar to the condition of the study area.

Fig. 5 shows that bed erosion is not considerable at the neap tide. It occurs only during a small portion of the tidal cycle. However, SSC is high and long-lasting during spring tide. Sediment movement, therefore, mainly occurs during spring tide when the current speed is high enough. The maximum turbidity and SSC at the ebb tide are much higher than the flood tide. Fig. 6 indicates that sediment suspension occurs when the current speed exceeds 45-55 cm.s-1.

Calibration parameters and their values for five simulation scenarios are listed in Table 5 as an example. Regarding the established criteria, each simulation scenario was selected based on the results of the previous one. Hence the model calibration was performed by a limited number of simulation scenarios. A comparison between the time series of simulated and measured SSC and current speed was carried out for each scenario.

Table 5. Calibration parameters and their values for selected simulation scenarios

Scenario	W_S (m/s)	Range of D_{50} (mm) corresponding to W_S *	τ_{cd} (N/m^2)	τ_{ce} (N/m^2)	Erosion Formula		Bed Roughness K_s (mm)	Sedimentation Rate in the Access Channel (m^3/month)
					E	n		
No. 4	0.004	[0.055-0.069]	0.05	0.07	0.00001	0.5	0.6	27500
No. 6	0.001	[0.028-0.033]	0.06	0.09	0.00001	0.7	0.6	21400
No. 8	0.01	[0.09-0.12]	0.07	0.1	0.00001	0.7	0.6	31300
No. 15	0.01	[0.09-0.12]	0.2	0.2	0.00001	0.7	1.2	30500
final	0.0025	[0.042-0.052]	0.15	0.3	0.000012	1.4	0.6	10100

* The column was added to compare measured grain size diameters (Table. 3) with the ones corresponding to settling velocity. Due to dependency of settling velocity to water temperature, a range of grain size corresponding to each settling velocity was given.

Considering the measured SSC (Table 2), it is expected that the maximum SSC during spring tide would be nearly 0.08 $kg.m^{-3}$ (the first criterion). According to Fig. 10-A, the maximum simulated SSC during spring tide for scenario No. 6 is about 0.2 $kg.m^{-3}$, which is more than the measured SSC. Fig. 10-B shows the same result for scenario No. 15 with maximum SSC equal to 0.05 $kg.m^{-3}$, which is less than the measured data.

The second criterion is related to the minimum turbidity at slack water during spring tide. Measured data (Fig. 5) show that this value is about 7% to 10% of the maximum turbidity. However, it does not drop to zero. If settling velocity is too low, the simulated SSC will not decrease as much as the measured values. Fig. 10-A (scenario No. 6) shows a situation where low settling velocity prevents SSC from falling as much as the observed values. The minimum SSC will drop to zero (Fig. 10-B) if the settling velocity is too high (like scenario No. 15). This demonstrates that settling velocity is the most crucial calibration parameter for the second criterion. It can also be inferred that critical bed shear stress for erosion is the main parameter to meet the third and fourth criteria. The fifth and sixth criteria are controlled using a velocity-SSC graph (see Fig. 6). The coefficient and the power of the erosion formula (Eq. (4)) can be determined from the velocity-SSC graph. The velocity-SSC graph is fairly sparse because of the effect of probability in suspension and deposition and the turbulence effects. The comparisons of measured and simulated velocity-SSC graphs for two non-calibrated scenarios (No. 4 and 8) are presented in Fig. 11. There is no satisfactory agreement between the measured and simulated critical velocity for erosion. It is also the case for the correlation coefficient between velocity and turbidity. An increase in the critical bed shear stress for deposition results in more sedimentation in the access channel. The rate of sedimentation in the access channel depends on (a) settling velocity and (b) the difference between critical bed shear stresses for erosion and deposition.

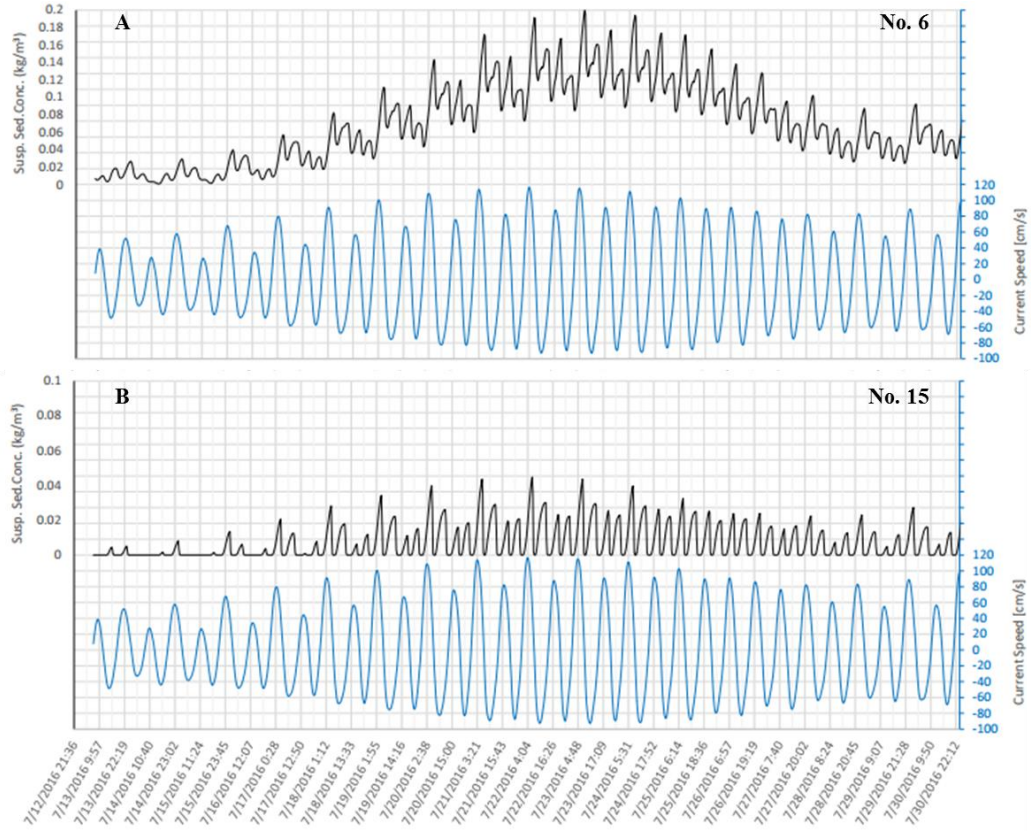

Fig. 10. The current speed and SSC time series for two non-calibrated scenarios (A: No. 6 and B: No. 15)

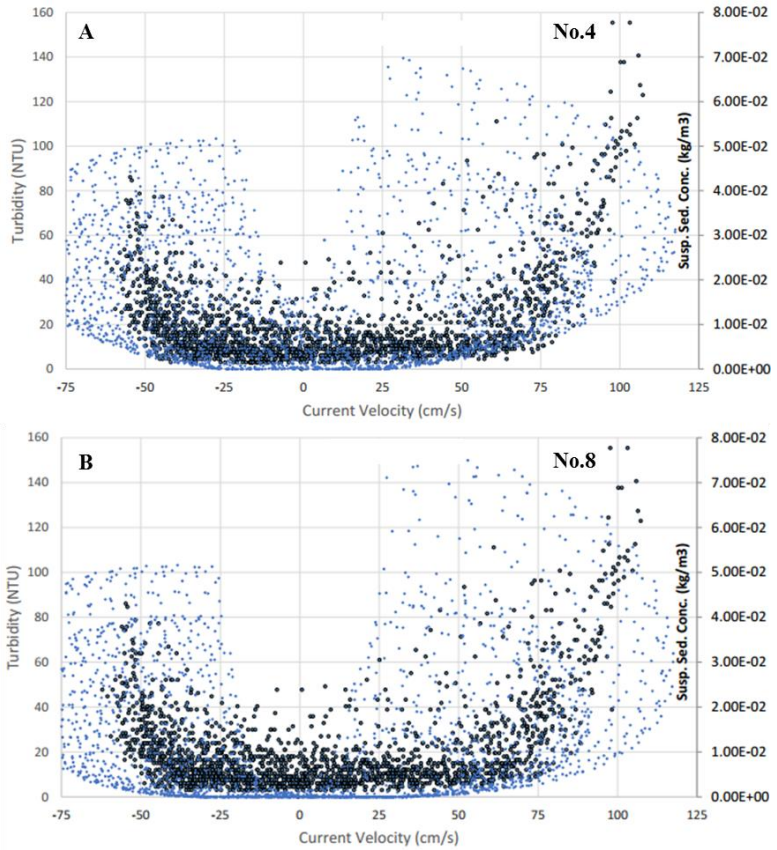

Fig. 11. The comparison of measured (the dark blue) and simulated (the light blue) velocity-SSC graph for two non-calibrated scenarios (A: No. 4 and B: No. 8)

5. Results and Discussion

The results of the calibrated model are depicted in Figs. 12 and 13. They confirm that the minimum current speed required for suspension is approximately 70 $cm.s^{-1}$ and 50 $cm.s^{-1}$ during ebb and flood tide, respectively, as validated by the measured data shown in Figs. 5 and 6. Furthermore, the maximum SSC during ebb tide is roughly twice that during flood tide. This indicates that the bed of each area is not only the source of the suspended sediment within that area, as the turbid water from upstream also contributes to the suspended sediment.

The maximum SSC during spring tide is about 0.08 $kg.m^{-3}$, while the maximum SSC during neap tide is approximately 0.02 $kg.m^{-3}$. This indicates that the tidal current makes sediment suspended just during spring tide. Therefore, the sedimentation process mainly occurs on spring tide days. Fig. 14 shows the instantaneous bed shear stress at ebb tide. It shows that the bed shear stress in the channel is less than the outside. This is due to the lower current speed in the channel. The

Fig. 15 demonstrates the erosion and deposition pattern at high and low-speed conditions, respectively. The current direction is nearly perpendicular to the access channel, because of the presence of natural trenches in the strait. The current velocity in the channel is less than the nearby area. Therefore, erosion in the channel is less than the outside at high speed current (Fig. 15-A). The duration of deposition in the channel is also longer than the outside area during each tidal cycle (Fig. 15-B). It results in a net deposition at each (spring) tidal cycle.

The calibrated model was used to estimate the deposition rate after deepening the channel. It estimated sedimentation in the access channel nearly with accuracy of 95% (122,000 m^3). The results also showed that deepening the channel from 15.5 to 19 meters leads to an increase in the deposition rate by about 80%. Both the simulation results and the measured data indicated that the maximum deposition takes place in the middle of the longitudinal direction of the channel and that erosion occurs near the harbor entrance (Fig. 16). This is in agreement with the results of Shanehsazzadeh and Ardalan [36] and Jafarzadeh Dehkordi, and Ershadi [37], who showed that the sedimentation mainly takes place in the mid one-third of Rajaee port access channel. It is worth noting that the current speed at the harbor entrance increases as the current is constricted into a narrower area, leading to erosion of the bed in that area.

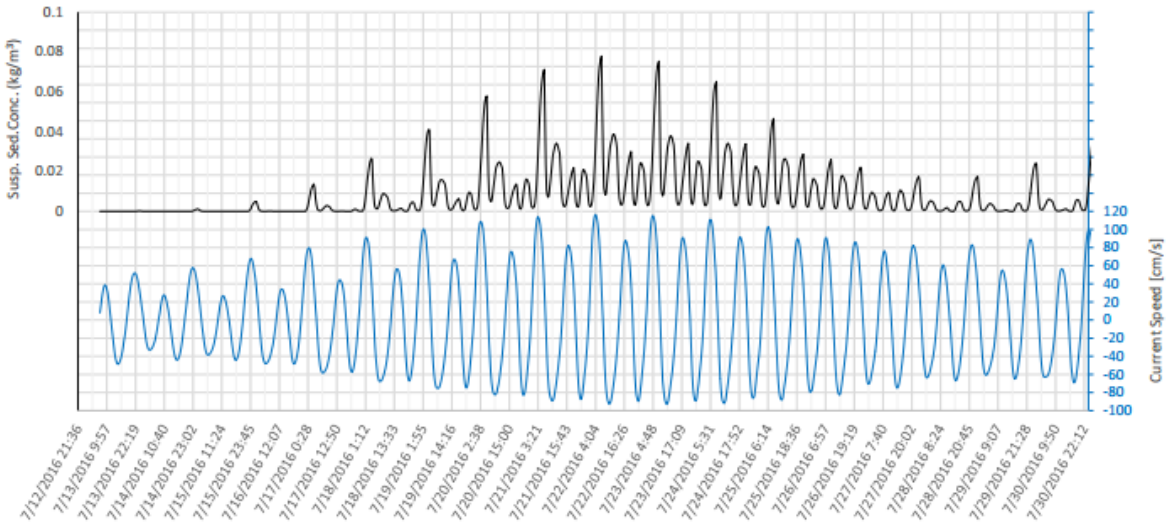

Fig. 12. The time series of current speed and SSC for the calibrated scenario (final)

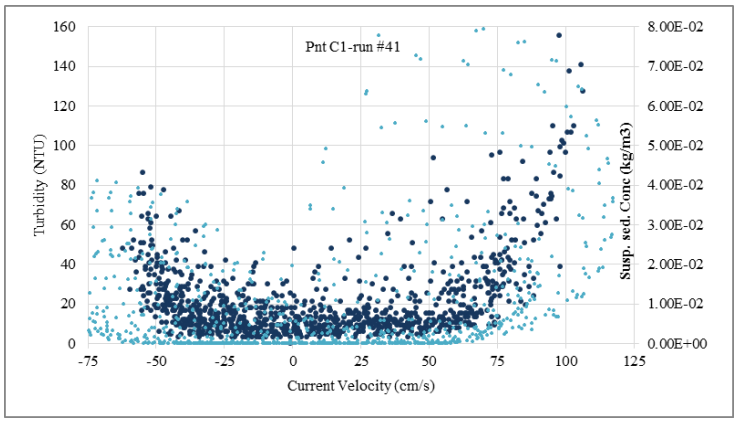

Fig. 13. The comparison of measured (the dark blue) and simulated (the light blue) velocity-SSC graph for the calibrated scenario (final)

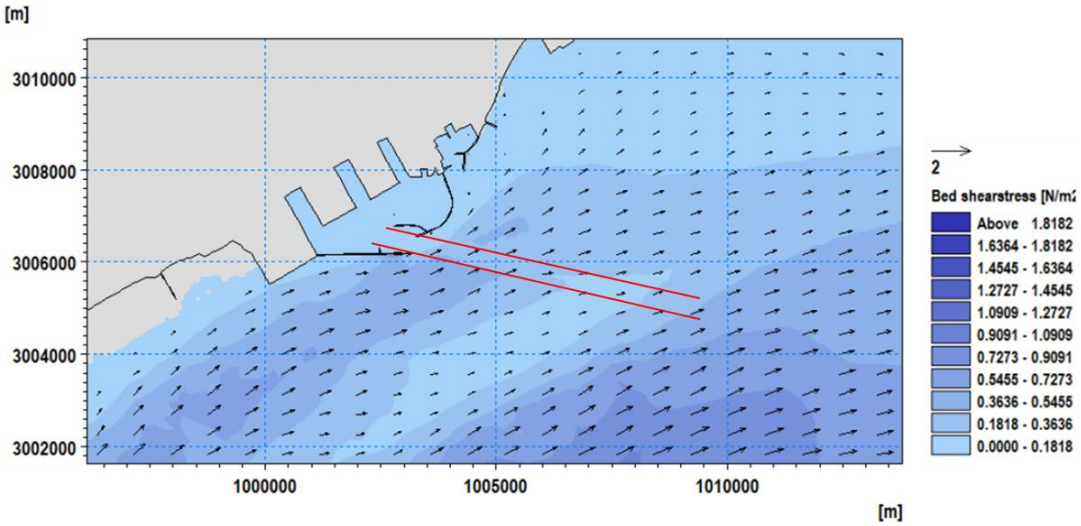

Fig. 14. Bed shear stress at a specific time at ebb tide

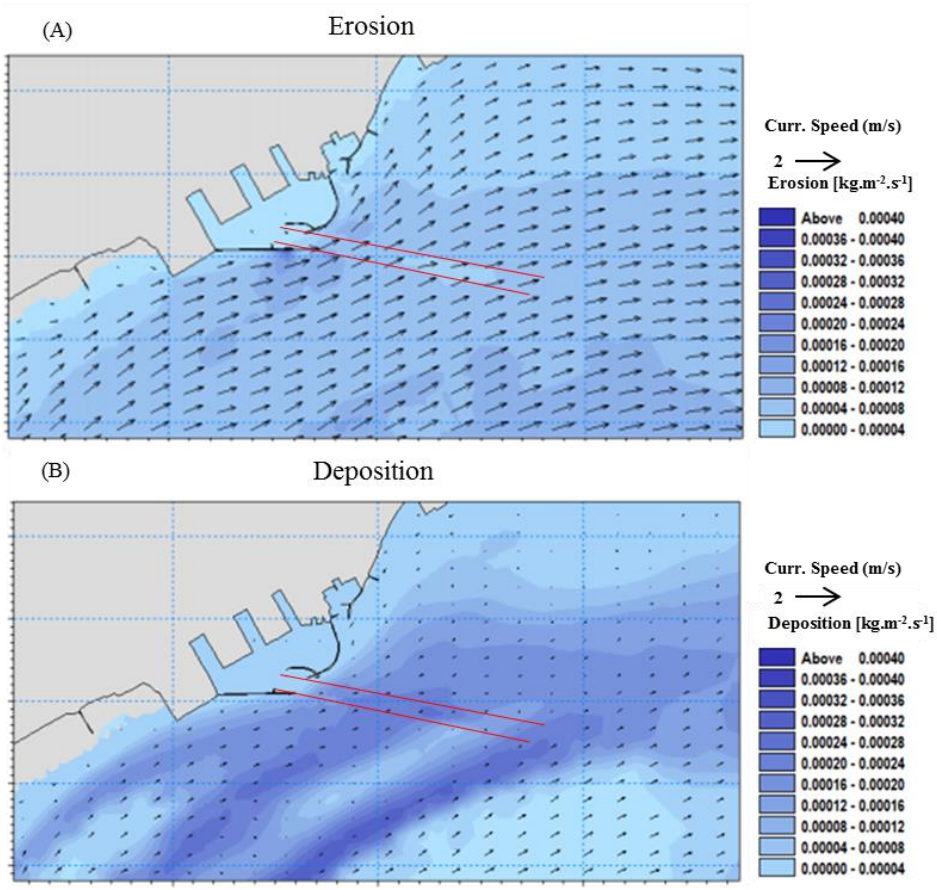

Fig. 15. Snapshots of the erosion at high speed (A) and deposition at low-speed conditions (B); red lines show the location of the access channel

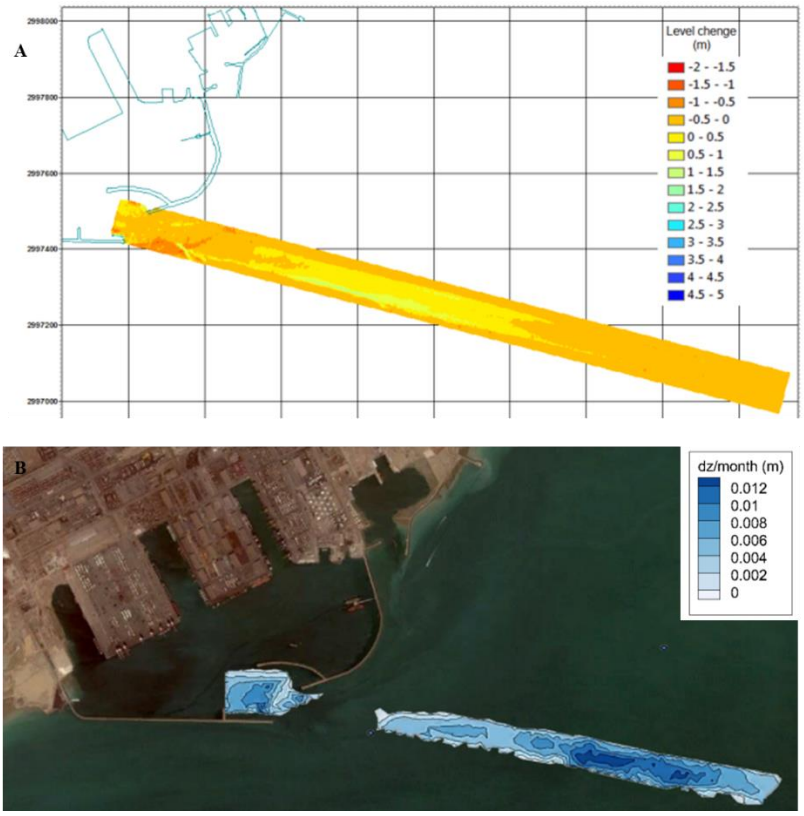

Fig. 16. Comparison of measured (up) [40] **and simulated (down) channel sedimentation rate**

6. Conclusion

A new procedure for effective model calibration in silt environments was presented. To this end, seven process-based criteria was proposed. The effect of calibration parameters on the criteria was evaluated for a real case study. The new procedure is suitable for conditions where limited amount of measured SSC data are available and helps model calibration to be performed with fewer simulation runs. The key point is the turbidity variation at different tidal conditions. The procedure was examined for a real case study (Shahid Rajaee Port). The results showed that the procedure could effectively calibrate the model. The calibrated model estimated the deposition rate in the access channel accurately.

The proposed algorithm can be automated in such a way that the critical bed shear stress for erosion, erodibility coefficient, and power of the erosion formula are determined using the scatter plot of velocity-SSC. Subsequently, the other parameters are automatically tuned using objective functions based on the criteria defined in this study. This approach is similar to the auto-calibration proposed by DHI [53], but with the criteria of the present study.

Acknowledgment

The authors acknowledge "Water Research Institute" and also "Port & Maritime Organization" for providing measured data. Support through DHI to access MIKE21/3 Coupled Model FM (in response to our request # 265562) is also gratefully acknowledged.

7. References

1. L. C. van Rijn, B. Grasmeijer and L. Perk, "Effect of Channel Deepening on Tidal Flow and Sediment Transport; Part I: Sandy Channels," Ocean Dynamics, vol. 68, pp. 1457-1479, 2018. doi: 10.1007/s10236-018-1204-2

2. L. C. van Rijn and B. Grasmeijer, "Effect of Channel Deepening on Tidal Flow and Sediment Transport; Part II: Muddy Channels," Ocean Dynamics, vol. 68, pp. 1481-1501, 2018. doi: 10.1007/s10236-018-1205-1

3. L. C. van Rijn, "Harbour Siltation and Control Measures," https://www.leovanrijn-sediment.com/papers/Harboursiltation2012.pdf, (2012, accessed 15 February 2021).

4. DHI, "MIKE 21 & MIKE 3 FLOW MODEL FM Mud Transport Module: Scientific Documentation," DHI, 2012.

5. Delft Hydraulics, "Delft3D-FLOW: Simulation of Multi-Dimensional Hydrodynamic Flows and Transport Phenomena, Including Sediments, User Manual," Deltares, Delft, Netherlands, 2014.

6. C. Chen, R. C. Beardsley, G. Cowles, J. Qi, Z. Lai, G. Gao, D. Stuebe, Q. Xu, P. Xue, J. Ge, S. Hu, R. Ji, R. Tian, H. Huang, L. Wu, H. Lin, Y. Sun and L. Zhao, "An Unstructured Grid, Finite-Volume Community Ocean Model FVCOM," Marine Ecosystem Dynamic Modeling Laboratory, 2013.

7. P. Tassi, T. Benson, D. Matthieu, J. Fontaine, N. Huybrechts, K. Rebekka, S. Pavan, C.-T. Pham, F. Taccone and W. Régis, "GAIA - a unified framework for sediment transport and bed evolution in rivers, coastal seas and transitional waters in the TELEMAC-MASCARET modelling system," Journal of Environmental Modelling & Software, vol. 159, 2022. doi.org/10.1016/j.envsoft.2022.105544

8. J. A. Roelvink and A. Reniers, A Guide to Modeling Coastal Morphology, World Scientific, Advances in Coastal and Ocean Engineering, 2011. doi: 10.1142/7712

9. S. A. Rahman and D. Chakrabarty, "Sediment Transport Modelling in an Alluvial River with Artificial Neural Network," Journal of Hydrology, vol. 588, 2020. doi: 10.1016/j.jhydrol.2020.125056

10. A. Yadav and P. Satyannarayana, "Multi-objective Genetic Algorithm Optimization of Artificial Neural Network for Estimating Suspended Sediment Yield in Mahanadi River Basin, India," International Journal of River Basin Management, vol. 18, no. 2, pp. 207-215, 2020. doi: 10.1080/15715124.2019.1705317

11. H. A. Arı Güner, I. Yüksel and E. Özkan Çevik, "Longshore Sediment Transport—Field Data and Estimations using Neural Networks, Numerical Model, and Empirical Models," Journal of Coastal Research, vol. 29, no. 2, pp. 311-324, 2013. https://doi.org/10.2112/JCOASTRES-D-11-00074.1

12. B. van Maanen, G. Coco, K. Bryan and B. Ruessink, "The Use of Artificial Neural Networks to Analyze and Predict Alongshore Sediment Transport," Nonlinear Processes in Geophysics, vol. 17, no. 5, pp. 395-404, 2010. doi: 10.5194/npg-17-395-2010

13. M. A. A. Almubaidin, S. Dashti Latif, K. Balan, A. N. Ahmed and A. El-Shafie, "Enhancing sediment transport predictions through machine learning-based multi-scenario regression models," *Results in Engineering*, vol. 20, 2023. doi.org/10.1016/j.rineng.2023.101585

14. M. S. Hanoon, A. A. Abdullatif B, A. N. Ahmed, A. Razzaq, A. H. Birima and A. El-Shafie, "A comparison of various machine learning approaches performance for prediction suspended sediment load of river systems: a case study in Malaysia," *Journal of Earth Science Information*, vol. 15, pp. 91-104, 2022. doi.org/10.1007/s12145-021-00689-0

15. H. Darabi, S. Mohamadi, Z. Karimidastenaei, O. Kisi, M. Ehteram, A. EL-Shafie and A. Torabi Haghighi , "Prediction of daily suspended sediment load (SSL) using new optimization algorithms and soft computing models," *Journal of Soft Computing:*

Methodologies and Application, vol. 25, pp. 7609-7626, 2021. doi.org/10.1007/s00500-021-05721-5

16. S. O. Sulaiman, M. F. Allawi, K. N. Sayl, M. Sherif and A. El-Shafie, "Suspended sediment load prediction modelling based on artificial intelligence methods: The tropical region as a case study," *Journal of Heliyon*, vol. 9, no. 8, 2023. doi.org/10.1016/j.heliyon.2023.e18506

17. F. Barzegari Banadkooki, M. Ehteram, A. N. Ahmed, F. Y. Teo, M. Ebrahimi, C. M. Fai, Y. F. Huang and A. El-Shafie, "Suspended sediment load prediction using artificial neural network and ant lion optimization algorithm," *Journal of Environmental Science and Pollution Research*, vol. 27, p. 38094–38116, 2020. doi.org/10.1007/s11356-020-09876-w

18. B. Lin and M. Montazeri Namin, "Modelling Suspended Sediment Transport using an Integrated Numerical and ANNs Model," Journal of Hydraulic Research, vol. 43, no. 3, pp. 302-310, 2005. doi: 10.1080/00221680509500124

19. K. Kaveh, M. D. Bui and P. Rutschmann, "Integration of Artificial Neural Networks into TELEMAC-MASCARET System, New Concepts for Hydromorphodynamic Modeling," Advances in Engineering Software, vol. 132, pp. 18-28, 2019. doi: 10.1016/j.advengsoft.2019.03.011

20. S. Bakshi and K. K. Bhar, "Simulation of Tidal Morpho-dynamics in the Hooghly Estuary using CMS Flow and Artificial Neural Network Models," in Procedia Computer Science, 2020. doi: 10.1016/j.procs.2020.03.255

21. U. Lumborg and A. Windelin, "Hydrography and Cohesive Sediment Modelling: Application to the Rømø Dyb Tidal Area," Journal of Marine Systems, vol. 38, no. 3-4, pp. 287-303, 2003. doi: 10.1016/S0924-7963(02)00247-6

22. U. Lumborg and M. Pejrup, "Modelling of Cohesive Sediment Transport in a Tidal Lagoon—an Annual Budget," Marine Geology, vol. 218, no. 1-4, pp. 1-16, 2005. doi: 10.1016/j.margeo.2005.03.015

23. J. F. Lopes, J. M. Dias and I. Dekeyser, "Numerical Modelling of Cohesive Sediments Transport in the Ria de Aveiro Lagoon, Portugal," Journal of Hydrology, vol. 319, no. 1-4, pp. 176-198, 2006. doi: 10.1016/j.jhydrol.2005.07.019

24. N. Margvelashvili, F. Saint-Cast and S. Condie, "Numerical Modelling of the Suspended Sediment Transport in Torres Strait," Continental Shelf Research, vol. 28, no. 16, pp. 2241-2256, 2008. doi: 10.1016/j.csr.2008.03.037

25. N. K. Ganju and D. H. Schoellhamer, "Calibration of an Estuarine Sediment Transport Model to Sediment Fluxes as an Intermediate Step for Simulation of Geomorphic Evolution," Continental Shelf Research, vol. 29, no. 1, pp. 148-158, 2009. doi: 10.1016/j.csr.2007.09.005

26. M. Xie, W. Zhang and W. Guo, "A Validation Concept for Cohesive Sediment Transport Model and Application on Lianyungang Harbor, China," Coastal Engineering, vol. 57, no. 6, pp. 585-596, 2010. doi: 10.1016/j.coastaleng.2010.01.003

27. L. H. Erikson, S. A. Wright, E. Elias , D. M. Hanes, D. H. Schoellhamer and J. Largier, "The Use of Modeling and Suspended Sediment Concentration Measurements for Quantifying Net Suspended Sediment Transport through a Large Tidally Dominated Inlet," Marine Geology, vol. 345, pp. 96-112, 2013. doi: 10.1016/j.margeo.2013.06.001

28. L. X. Tu, V. Q. Thanh, J. Reyns, S. P. Van, D. T. Anh, T. D. Dang and J. A. Roelvink, "Sediment Transport and Morphodynamical Modeling on the Estuaries and Coastal Zone of the Vietnamese Mekong Delta," Continental Shelf Research, vol. 186, pp. 64-76, 2019. doi: 10.1016/j.csr.2019.07.015

29. J. Chang, G.-h. Lee , C. K. Harris, Y. Song, S. M. Figueroa, N. W. Schieder and K. D. Lagamayo, "Sediment Transport Mechanisms in Altered Depositional Environments of the Anthropocene Nakdong Estuary: A Numerical Modeling Study," Marine Geology, vol. 430, 2020. doi: 10.1016/j.margeo.2020.106364

30. Z. Y. Xiao, X. H. Wang, D. Song, I. Jalon-Rojas and D. Harrison, "Numerical Modelling of Suspended Sediment Transport in a Geographically Complex Microtidal Estuary: Sydney Harbour Estuary, NSW," Estuarine, Coastal and Shelf Science, vol. 236, 2020. doi: 10.1016/j.ecss.2020.106605

31. L. Zhua, W. Gonga, H. Zhang, W. Huang and R. Zhang, "Numerical Study of Sediment Transport Time Scales in an Ebb-dominated Waterway," Journal of Hydrology, vol. 591, 2020. doi: 10.1016/j.jhydrol.2020.125299

32. J. Allen, P. Somerfield and F. Gilbert, "Quantifying Uncertainty in High-resolution Coupled Hydrodynamic-ecosystem Models," Journal of Marine Systems, vol. 64, no. 1-4, pp. 3-14, 2006. doi: 10.1016/j.jmarsys.2006.02.010

33. S. Orseau, N. Huybrechts, P. Tassi, D. P. Van Bang and F. Klein, "Two-dimensional modeling of fine sediment transport with mixed sediment and consolidation: Application to the Gironde Estuary, France," *International Journal of Sediment Research*, vol. 36, no. 6, pp. 736-746, 2021. doi.org/10.1016/j.ijsrc.2019.12.005

34. L. P. Bitencourt, E. H. Fernan, P. D. da Silva and O. Moller Jr, "Spatio-temporal variability of suspended sediment concentrations in a shallow and turbid lagoon," *Journal of Marine Systems*, vol. 212, 2020. doi.org/10.1016/j.jmarsys.2020.103454

35. H. d. O. Fagundes, F. M. Fan and R. C. D. de Paiva, "Automatic Calibration of a Large-scale Sediment Model using Suspended Sediment Concentration,

Water Quality, and Remote Sensing Data," Journal of Revista Brasileira de Recursos Hidricos (RBHR), vol. 24, no. 10, 2019. https://doi.org/10.1590/2318-0331.241920180127

36. A. Shanehsazzadeh and H. Ardalan, "Regional-Scale Study on Sediment Processes of Khuran Strait at Persian Gulf with Implications for Engineering Design," *China Ocean Engineering*, vol. 33, no. 3, pp. 356-364, 2019. DOI: 10.1007/s13344-019-0034-4

37. E. Jafarzadeh Dehkordi and C. Ershadi, "Numerical Modeling of Current Pattern and Sediment Transport in Access Channel of Shahid Rajaei Port," Journa of Maritime Transport Industry, vol. 5, no. 4, pp. 34-40, 2020. doi: 10.30474/jmti.2020.104359

38. P. V. Lisboa, E. H. Fernandes, A. Sottolichio, N. Huybrecht, A. R. Rodrigues Bendô and J. Costi, "Bottom Evolution Patterns driven by hydrodynamic forcing in the Southwest Atlantic Inner Continental Shelf, off Río de la Plata and Patos Lagoon," *Jornal of Continental Shelf Research*, vol. 225, 2023. doi.org/10.1016/j.csr.2023.104934

39. UK Hydrographic Office, "Admiralty Tide Tables Vol3," UK Hydrographic Office, 2016.

40. Fara Darya Arsheh Consultants and Sogreah Consultants, "Monitoring and Modelling Study of Iranian Coasts Project; Phase 4; Hormozgan; Yearly Report of Field Measurement," Port & Maritime Organization, 2012.

41. Tehran Berkeley Group of Companies, "Shahid Rajaee Port Complex Development Plan Project; Phase 3; Sedimentation Inside the Access Channel Final Report," Port & Maritime Organization, 2018.

42. M. E. W. E. Consultants, "Investigation of Sedimentation in the Harbour Basins and Access Channels- Shahid Rajaee Port," Port & Maritime Organization, 2012.

43. Water Research Institute, "Bandar Abbas Gas Refinery Project; Cooling Water Intake Studies; Field Measurement Final Report," Persian Gulf Star Oil Company, 2007.

44. Y. Wang, Y. Peng, Z. Du, H. Lin and Q. Yu, "Calibrations of Suspended Sediment Concentrations in High-Turbidity Waters Using Different In Situ Optical Instruments," Jornal of Water, vol. 12, no. 11, 2020. doi:10.3390/w12113296

45. U.S. Geological Survey, "Relations Between Continuous Real-Time Turbidity Data and Discrete Suspended Sediment Concentration Samples in the Neosho and Cottonwood Rivers,East-Central Kansas, 2009–2012," USGS Science for a changing world, 2014.

46. H. Marttila and B. Kløve, "Use of Turbidity Measurements to Estimate Suspended Solids and Nutrient Loads from Peatland Forestry Drainage," Journal of Irrigation and Drainage Engineering, vol. 138, no. 12, pp. 1088-1096, 2012. https://doi.org/10.1061/(ASCE)IR.1943-4774.0000509

47. C. A. Ellison, R. L. Kiesling and J. D. Fallon, "Correlating Streamflow, Turbidity, and Suspended-Sediment Concentration in Minnesota's Wild Rice River," in 2nd Joint Federal Interagency Conference, Las Vegas, 2010.

48. E. Patault, C. Alary, C. Franke, A. Gauthier and N. Abriak, "Assessing Temporal Variability and Controlling Factors of the Sediment Budget of a Small Agricultural Catchment in Northern France (the Pommeroye)," Journal of Heliyon, vol. 5, no. 3, 2019. https://doi.org/10.1016/j.heliyon.2019.e01407

49. J. Downing, "Twenty-five Years with OBS Sensors: The Good, The Bad, and The Ugly," Journal of Continental Shelf Research, vol. 26, no. 17-18, pp. 2299-2318, 2006. https://doi.org/10.1016/j.csr.2006.07.018

50. E. Skarbøvik, S. Gyritia, M. vant Veen, E. E. Lannergård, H. Wenng, M. Stutter, M. Bieroza, K. Atcheson, P. Jordan, J. Fölster, P.-E. Mellander, B. Kronvang, H. Marttila, Ø. Kaste, A. Lepistö and M. Kämäri, "Comparing in situ Turbidity Sensor Measurements as a Proxy for Suspended Sediments in North-Western European Streams," Journal of CATENA, vol. 225, 2023. https://doi.org/10.1016/j.catena.2023.107006

51. L. F. Murillo-Bermúdez, A. L. S. Salustiano-Martim, C. Poleto and J. G. Dalfré Filho , "Correlation of Turbidity and Suspended Sediment Concentration in Natural Water Flow using Alternative Data of Water Treatment Plant, Case of Study in the Upper Jundiaí River, Brazil," International Journal of River Basin Management, vol. 21, no. 2, pp. 233-241, 2023. https://doi.org/10.1080/15715124.2021.1961794

52. L. Dalbianco, R. Ramon, C. A. P. de Barros, J. P. G. Minella, G. H. Merten and E. J. Didoné, "Sampling Strategies to Estimate Suspended Sediment Concentration for Turbidimeter Calibration," Jornal of Revista Brasileira de Recursos Hidricos (RBHR), vol. 21, no. 12, pp. 884-889, 2017. https://doi.org/10.1590/1807-1929/agriambi.v21n12p884-889

53. DHI, "Auto Calibration Tool: User Guide," DHI, 2012.